# TRUSS WAVINESS EFFECTS IN CELLULAR LATTICE STRUCTURES

Douglas T. Queheillalt, Vikram S. Deshpande and Haydn N. G. Wadley

# TRUSS WAVINESS EFFECTS IN CELLULAR LATTICE STRUCTURES

DOUGLAS T. QUEHEILLALT, VIKRAM S. DESHPANDE AND HAYDN N. G. WADLEY

Methods have emerged for making metallic lattice structures either by the lay up of collinear wire arrays or by stacking woven textile meshes. The two fabrication routes result in similar lattice topologies: the collinear lattice has straight struts while those in the textile lattice are wavy. Wire waviness in the textile lattice results in a knockdown in both the stiffness and strength compared to the collinear lattice. Analytical estimates and finite element (FE) predictions of the through thickness compressive responses of collinear and textile lattices indicate that the stiffness and strength of lattices oriented to form a diamond structure are specimen aspect ratio dependent. By contrast, the stiffness of the collinear and textile lattices oriented to form a square structure is independent of both specimen aspect ratio and height while the strength depends on the sandwich height. Experimental measurements on specimens fabricated from 304L stainless steel are in good qualitative agreement with the elastic ideally-plastic analytical estimates while FE predictions incorporating the full strain hardening response of the parent material give accurate quantitative predictions of the measurements.

## 1. Introduction

Lightweight metallic sandwich panel structures that utilize low density cores and solid face sheets are widely used in aerospace and other transportation applications where high specific stiffness and/or strength is required. Hexagonal honeycomb structures are frequently used for the cores of sandwich panels [Bitzer 1997]. However, sandwich panels with metal foam cores, which might be structurally less efficient, are also of interest as they facilitate various multifunctional applications [Ashby et al. 2000]. The lower specific strength of metal foam cores is a consequence of the fact that their stiffness and strengths are primarily governed by bending of the constituent struts and cell walls and thus scale as $\bar{\rho}^2$ and $\bar{\rho}^{1.5}$, respectively, where $\bar{\rho}$ is the relative density [Gibson and Ashby 1997]. In contrast, the stiffness and strength of lattice materials are governed by the stretching of the constituent struts and scale with $\bar{\rho}$ [Deshpande and Fleck 2001]. It follows that a *stretching-dominated* cellular material with $\bar{\rho} = 0.1$ is predicted to be about ten times stiffer and about three times stronger than the equivalent relative density (weight) foam [Deshpande and Fleck 2001].

A variety of stretching-dominated cellular metal topologies have recently been proposed for cores of sandwich panels, and simple methods for their fabrication from high performance alloys have been identified, as reviewed by Wadley et al. [2003]. These include pyramidal, tetrahedral and Kagomé lattice trusses [Deshpande and Fleck 2001; Sypeck and Wadley 2002; Hyun et al. 2003; Wang et al. 2003;

Kooistra et al. 2004; Zok et al. 2004], the prismatic diamond lattice [Valdevit et al. 2004; Cote et al. 2006] and a square-honeycomb lattice [Berggren et al. 2001; Cote et al. 2004; Meidell 2005; Liang and Chen 2006]. Besides these recent examples, there exist well established theories for analyzing sandwich panels. The reader is referred to [Noor et al. 1995; Buannic et al. 2003] and the references therein for additional information regarding computational modeling of sandwich panels and shells. Simple brazing methods can also be used to bond together metallic wire meshes resulting in periodic metal lattice structures with a woven or textile topology [Sypeck and Wadley 2001; Zupan et al. 2004]. These structures can then be cut and brazed to facesheets resulting in sandwich structures. The lattice core structures can be oriented such that they have their struts aligned parallel-to and perpendicular-to the sandwich panel facesheets (a square orientation) or rotated at say ±45° to the faces (a diamond orientation). Recently, a method for fabricating a cellular lattice structure with an analogous topology using collinear arrays of solid wires or hollow tubes has also been reported [Queheillalt and Wadley 2005]. From a mechanics perspective, the main difference between the two topologies is that while the textile lattice is comprised of wavy wires, the collinear lattice consists of straight struts. This study explores the consequences of waviness on the mechanical properties of these similar topologies.

The effects of various structural defects or imperfections on the mechanical properties of regular honeycomb and bending-dominated foam structures have been extensively investigated using a combination of finite element and analytical techniques. Simone and Gibson [1998b], Grenestedt and Tanaka [1998], and Grenestedt and Bassinet [2000] reported that plateau borders (cell walls with a nonuniform wall thickness) had only a minor effect on the mechanical properties of hexagonal honeycombs and closed-cell foams with tetrakaidecahedral cells. On the other hand, Grenestedt [1998], Simone and Gibson [1998a], Chen et al. [1999], and Grenestedt and Bassinet [2000] found that wavy cell walls significantly reduce both the Young's modulus and compressive yield strength of cellular materials.

Strut waviness is also expected to play a role in determining the mechanical properties of the stretching-dominated textile and collinear lattice materials. However, limited data is available on the effects of defects on the strength of lattice materials. Wallach and Gibson [2001] used finite element methods to look at the effect of randomly removing truss members of an *octet* truss structure. They determined that both the Young's modulus and strength in compression decrease linearly ∼15–20% after randomly removing only 10% of the constituent struts. Here we use analytical, finite element, and experimental techniques to investigate the through thickness compressive response of collinear and textile lattices with cores oriented in both a diamond and square orientation. The issues of specimen size dependent mechanical properties and the influence of strut waviness in these sandwich core materials are addressed.

## 2. Analytical mechanical property relationships

Four lattices of interest have been identified based on two orientations of brazed collinear and textile materials configured as the core of a sandwich structure (Figure 1): (i) collinear lattice in a diamond orientation; (ii) collinear lattice in a square orientation; (iii) textile lattice in the diamond orientation; and (iv) textile lattice in the square orientation.

The schematic illustrations in Figure 1 indicate that while the topology of the collinear and textile lattices are similar, the collinear lattices consist of straight struts (Figure 1(a) and (b)), while the textile lattices have wavy struts with a peak-to-peak amplitude equal to the wire diameter (Figures 1(c) and 1(d)).

We also note that the angle of inclination of the struts in a diamond orientation is $\omega = \pm 45°$ ($x_1 - x_2$ plane) with respect to the sandwich faces and are $0°$ and $90°$ for the square orientation.

Neglecting the added mass of braze material used during fabrication, geometrical considerations give the relative density, $\bar{\rho}$, of the collinear and textile lattice materials (to first order in $a/l$) as

$$\bar{\rho} = \frac{\pi}{2 \sin 2\omega}\left(\frac{a}{l}\right), \tag{1}$$

where $\omega$ is the half weave angle, $a$ is the radius of the wire strut, and $l$ is the cell size (center-to-center wire spacing) as defined in Figure 1(a).

**2.1.** *Diamond orientation.* Approximate analytical expressions have been developed for the through thickness compressive stiffness and strength of lattices made from an elastic ideally-plastic solid material with a Young's modulus $E_s$, Poisson's ratio $v$ and yield strength $\sigma_{ys}$ [Sypeck and Wadley 2001; Zupan et al. 2004]. We begin by reviewing expressions for the stiffness and strength of a collinear (nonwavy) structure and then modify these expressions to account for the waviness of the wires in the textile structure.

**2.1.1.** *Collinear lattice.* Consider a sandwich plate of length $L$ with rigid facesheets and a collinear diamond lattice core of thickness $H$ (Figure 1). Note that in the diamond orientation, some of the struts are attached to both facesheets while near the edge of the sandwich panel; some of the struts are attached to only one of the facesheets. Zupan et al. [2004] derived lower bound estimates for the mechanical properties of such a structure loaded in the through thickness direction. In their derivation, they assumed
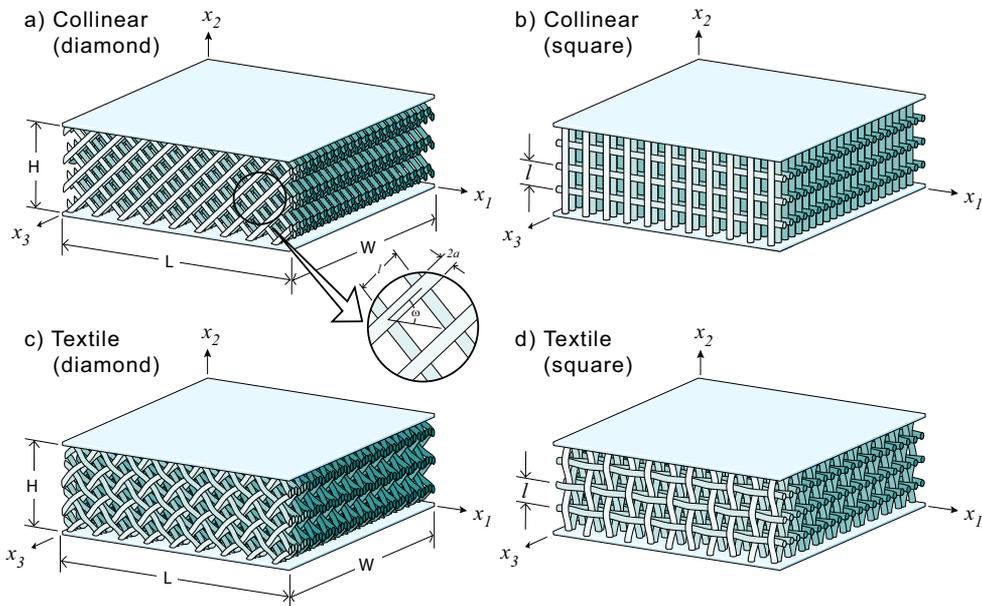


**Figure 1.** Schematic illustrations of (a) the collinear core in the diamond orientation, (b) the collinear core in the square orientation, (c) the textile core in the diamond orientation and (d) the textile core in the square orientation.

that wires attached to only one facesheet carried no load (i.e. do not contribute to the mechanical response) while wires attached to both facesheets are subject to an axial stress, $\sigma_f$, established by equilibrium with an applied macroscopic compressive stress in the $x_2$-direction. Using this approach, they showed that the normalized Young's modulus $E$ of the lattice is given by

$$\frac{E}{E_s} = \left(1 - \frac{1}{A \tan \omega}\right) \sin^4 \omega \cdot \bar{\rho}, \tag{2}$$

where $A \equiv L/H$ is the aspect ratio of the sandwich plate. Note that the term $1 - 1/A \tan \omega \rightarrow 1$ as $A \rightarrow \infty$ and the normalized Young's modulus of the lattice asymptotically reaches a maximum of $E/E_s = \sin^4 \omega \cdot \bar{\rho}$ for samples that are long compared to their thickness. In other words, edge effects due to the struts that are attached to only one facesheet become negligible. Note also that deformation in the $x_3$ direction has been neglected in this analysis and thus Equation (2) is accurate for $W \gg H$.

The yield strength $\sigma$ of the lattice can similarly be determined directly from equilibrium conditions [Zupan et al. 2004]. It is assumed that each strut attached to both facesheets is at the yield point, and the macroscopic compressive yield strength of the lattice in the $x_2$-direction is given by

$$\frac{\sigma}{\sigma_{ys}} = \left(1 - \frac{1}{A \tan \omega}\right) \sin^2 \omega \cdot \bar{\rho}. \tag{3}$$

Again, it should be noted that Equations (2) and (3) neglect the contribution to the stiffness and strength from bending of the constituent wires: these contributions become increasingly important for small aspect ratio specimens and thus Equations (2) and (3) are expected to underpredict the stiffness and strength of sandwich structures with low values of $A$.

The collinear lattice collapses by elastic buckling of the constituent struts if the Euler buckling load $P_{\text{euler}}$ of the constituent struts is less than or equal to their plastic yield strength. The Euler buckling load of a cylindrical column is given by

$$P_{\text{euler}} = \frac{k^2 \pi^3 E_s a^4}{4l^2}, \tag{4}$$

while the plastic yield load $P_{\text{yield}} = \pi a^2 \sigma_{ys}$. The factor $k$ in Equation (4) depends on the rotational stiffness of the end nodes of the strut. The lowest strength buckling mode under uniaxial compression corresponds to struts of length $l$ buckling as pin-ended (freely rotating) struts as sketched in Figure 2(c). Thus, we take $k = 1$ in Equation (4) and it follows that the collinear lattice collapses by elastic buckling of the constituent struts if the relative density

$$\bar{\rho} \le \frac{1}{\sin 2\omega} \sqrt{\varepsilon_y}, \tag{5}$$

where the yield strain $\varepsilon_y \equiv \sigma_{ys}/E_s$. In the regime of relative densities where elastic buckling dominates, the collapse strength is given by

$$\frac{\sigma}{\sigma_{ys}} = \frac{1}{\varepsilon_y}\left(1 - \frac{1}{A \tan \omega}\right) \sin^2 \omega \cdot \bar{\rho}^3. \tag{6}$$
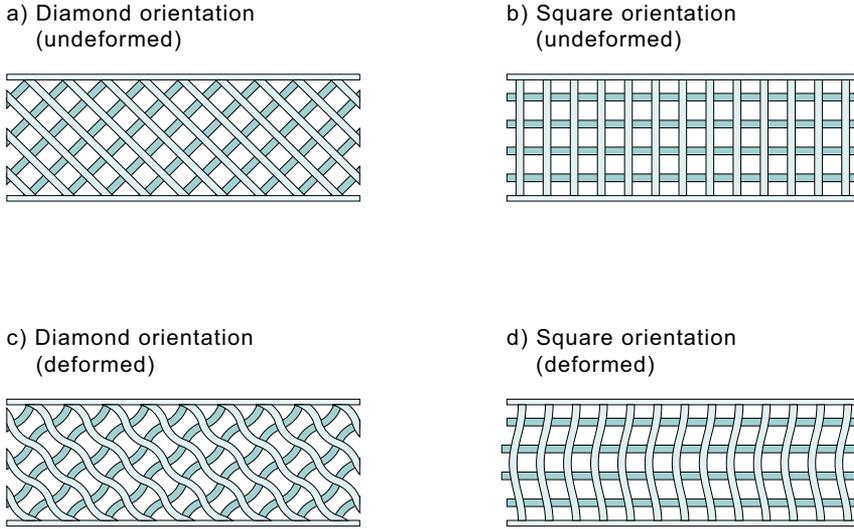
**Figure 2.** Sketches of the buckling modes of the collinear and textile sandwich cores in the diamond and square orientations.

**2.1.2.** *Textile lattice.* Unlike the collinear lattice, the wires in a textile are wavy with the transverse (in the $x_3$-direction) profile $w(s)$ of each wire approximated by

$$w = a\left(1 - \cos\frac{\pi s}{l}\right), \tag{7}$$

where $s$ is the axial coordinate along one strut of a cell measured from a node. This waviness results in a reduction in the axial stiffness and load carrying capacity of each wire and thus the textile lattice is anticipated to have a lower stiffness and strength compared to an equivalent collinear lattice material.

We first analyze the effective stiffness and strength of a long wavy wire as sketched in Figure 3(a). The transverse profile of this wire is assumed to be described by Equation (7). The supports in Figure 3(a) prevent the transverse deflection (in the $x_3$-direction) of the wire and represent the constraint imposed by successive layers of the wire meshes which are all brazed together at the nodes. A free-body diagram of a wire segment between two supports is sketched in Figure 3(b), where $P$ is the applied axial load and $R$ the horizontal reaction from the supports. Antisymmetry considerations dictate that the bending moment vanishes at the supports. Thus, moment equilibrium implies that

$$R = 2P\left(\frac{a}{l}\right). \tag{8}$$

For $a/l \ll 1$, we can assume that the axial load $P$ and shear force $R$ are approximately constant through the length of the strut. Then the total elastic strain energy, $U$, in a wavy strut of length $l$ is given by the sum of the stretching, bending and shearing energies

$$U = \frac{1}{2E_s}\frac{P^2 l}{\pi a^2} + \frac{1}{2}\int_0^l \frac{M^2}{E_s I}ds + \frac{1+\nu}{E_s}\frac{R^2 l}{\pi a^2}, \tag{9}$$
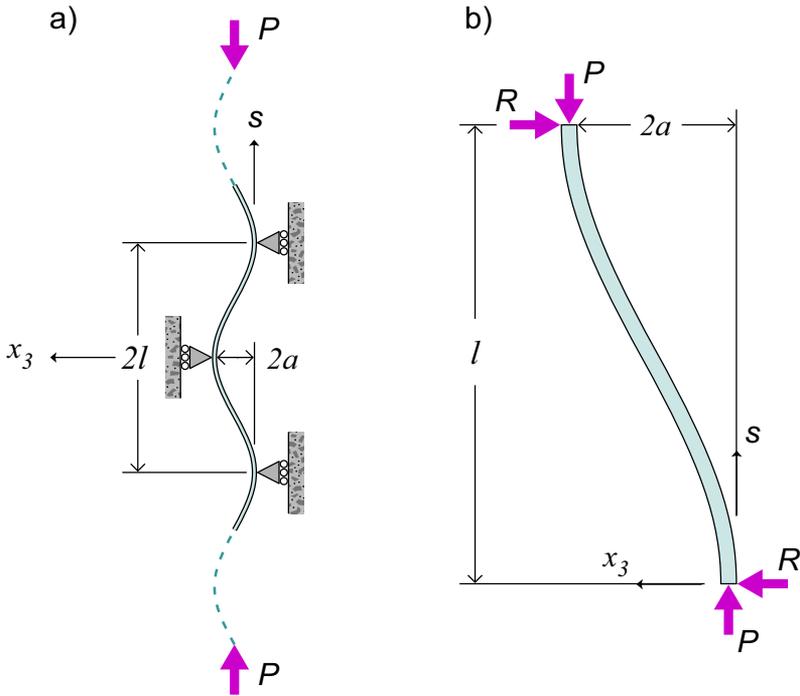
**Figure 3.** (a) Sketch of the loading on a single wavy wire in the textile core and (b) a free-body diagram of the representative wavy wire.

where the bending moment

$$M(x) = Pa\left(1 - \cos\frac{\pi s}{l}\right) + Pa\left(\frac{a}{l}\right)s, \tag{10}$$

and the second moment of area of the cylindrical wire $I = \pi a^4/4$.

A work balance gives the effective modulus $E_w$ of the wavy strut as

$$\frac{E_w}{E_s} = \frac{1}{1.09 + 8(1+\nu)\left(\frac{a}{l}\right)^2}. \tag{11}$$

Note that the decrease in $E_w$ with increasing $a/l$ is a result of the contribution of shear deflections to the compliance of the wavy struts.

The yield locus of a beam element under combined bending and tension is given by (see for example [Prager 1959])

$$\left(\frac{P}{P_o}\right)^2 + \left(\frac{M}{M_o}\right) = 1, \tag{12}$$

where for a strut of circular cross-sectional radius $a$, $P_o = \pi a^2 \sigma_{ys}$ and $M_o = 4a^3\sigma_{ys}/3$. Since the axial load is constant through the strut length, yielding of the strut is expected to commence at the point of

maximum bending moment. Equation (10) dictates that the maximum bending moment is

$$M_{\max} = \left[ \left( 1 - \sqrt{1 - \frac{4}{\pi^2}} \right) - \frac{2}{\pi} \sin^{-1}\left(\frac{2}{\pi}\right) \right] \cdot Pa = \lambda Pa, \tag{13}$$

and thus the collapse stress $\sigma_w$ of the wavy strut follows from the yield locus, Equation (12), as

$$\frac{\sigma_w}{\sigma_{ys}} = \frac{\pi\lambda + \sqrt{\pi^2\lambda^2 + 64/9}}{8/3}. \tag{14}$$

The normalized modulus and plastic yield strength of the textile sandwich lattice material may then be estimated by replacing $E_s$ and $\sigma_{ys}$ by $E_w$ and $\sigma_w$, respectively, in Equation (2) and Equation (3). The effect of strut waviness on the elastic buckling strength of the textile material is not explored in detail here. However, as the wires buckle as pin-ended struts in the plane of each wire mesh, the wavy imperfections in the $x_2 - x_3$ plane are expected to have only a minor effect upon the elastic buckling strength of the textile sandwich lattice [Zupan et al. 2004].

**2.2. Square orientation.** In this section, we derive approximate formulae for the Young's modulus and compressive strength of the collinear and textile lattices in the square orientation. The lattices are again assumed to be made from an elastic ideally-plastic solid material with a Young's modulus $E_s$ and yield strength $\sigma_{ys}$.

**2.2.1.** *Stiffness.* Under out-of-plane compression (in the $x_2$-direction), only the vertical wires carry load and the normalized Young's modulus of the collinear sandwich lattice is given by

$$\frac{E}{E_s} = \frac{\pi}{4}\left(\frac{a}{l}\right) = \frac{\bar{\rho}}{2}. \tag{15}$$

The Young's modulus of the textile material is obtained by replacing $E_s$ in the above equation with $E_w$ from Equation (11).

**2.2.2.** *Strength.* The horizontal wires do not contribute to the compressive strength of the sandwich lattices in the square orientation. Assuming that vertical wires (aligned along the $x_2$-direction) undergo compressive yield, the effective yield strength of the collinear lattice follows as

$$\frac{\sigma}{\sigma_{ys}} = \frac{\pi}{4}\left(\frac{a}{l}\right) = \frac{\bar{\rho}}{2}, \tag{16}$$

while the strength of the textile lattice is obtained by replacing $\sigma_{ys}$ in the above equation with $\sigma_w$ from Equation (14).

In the square orientation, experimental studies [Queheillalt and Wadley 2005] indicate the lattice collapses by cooperative Euler buckling of the constituent struts over the full height of the sandwich; see Figure 2. Assuming that the struts are built into the sandwich faces, the elastic buckling collapse load of a square lattice made from either the collinear or textile materials is given by

$$\frac{\sigma}{\sigma_{ys}} = \frac{\pi^3}{4\varepsilon_y}\left(\frac{a}{l}\right)^3\left(\frac{l}{H}\right)^2 = \frac{2\bar{\rho}^3}{\varepsilon_y}\left(\frac{l}{H}\right)^2, \tag{17}$$

where we have assumed that the waviness of the trusses in the textile lattice does not substantially affect the elastic buckling loads of the trusses. Comparing Equation (16) and Equation (17), we see that elastic buckling is the operative collapse mode for lattice relative densities satisfying the inequality

$$\bar{\rho}^2 < \frac{\pi^2 \varepsilon_y}{4} \left(\frac{H}{l}\right)^2. \tag{18}$$

It is important to note that the elastic buckling strength of the sandwich lattice materials in the square orientation is not an intrinsic material property; it decreases with increasing lattice height for a fixed value of the relative density.

## 3. Finite element simulations

The analytical expressions for the stiffness and strength of the lattice materials in the diamond orientation is checked by performing finite element (FE) calculations with the general purpose finite element package ABAQUS. Here the intent is only to compare the FE and analytical predictions and not study a specific parent material. In these FE calculations, the collinear and textile materials were rigidly jointed at the nodes and hence the FE calculations include contributions from the bending of the struts, which were neglected in the analytical calculations. We note that the compression of the square lattice is simply equivalent to the uniaxial compression of the vertical trusses and hence excellent agreement between the FE and analytical calculations was obtained and for the sake of brevity those comparisons are omitted here.

Two types of FE calculations were performed for both the collinear and textile lattices with a diamond topology:

- periodic unit cell calculations to determine the effective properties of the lattice materials,
- calculations on a sandwich beam with a finite aspect ratio.

The waviness of the mesh wires in the textile material was assumed to be of the form specified by Equation (7) with each wire modeled using 3-dimensional Timoshenko beam elements (B32 element in the ABAQUS notation) of size $l/20$. At each node of the cellular material (the wire crossover points), no relative displacement or rotation of one wire with respect to the other was permitted. This models a rigidly brazed joint. To reduce the size of the computations, only one layer of the wire mesh was modeled in the FE calculations with symmetry boundary conditions (i.e. displacement $u_3 = 0$ and the rotations $\theta_1 = \theta_2 = 0$) imposed on the nodes (wire crossover points) of the cellular material. Thus, the FE calculation models a plane strain limit which is valid for a cellular material comprising a large number of wire mesh layers with $W \gg H$. The FE models for the collinear material were essentially the same as those of the textile material, except that the wire waviness term was set to zero in this case. Imperfections were not included in the $x_1 - x_2$ plane in the FE calculations as the large waviness in the $x_3$-direction dominates the buckling strength of the struts of these textile cores.

In the linear elastic calculations used to determine the Young's modulus, the solid wire material was modeled as linear elastic with a Poisson's ratio $\nu = 0.3$. For the strength calculations, the solid material was assumed to be a J2 flow theory elastic ideally-plastic solid with a yield strain $\varepsilon_y = 0.5\%$ and an elastic Poisson's ratio $\nu = 0.3$.

**3.1.** *Effective properties of the infinite material.* In order to determine the effective properties of the collinear and textile lattice materials, a unit cell of the material was analyzed in the FE calculations. Periodic boundary conditions were specified through

$$\Delta u_i = \bar{\varepsilon}_{ij} \Delta x_j \qquad \text{and} \qquad \Delta \theta_i = 0, \tag{19}$$

where $\Delta u_i$ and $\Delta \theta_i$ are the differences in the displacements and rotations on opposites sides of the unit cell specified by the position difference vector $\Delta x_j$. Here we consider compression in the $x_2$-direction and thus specify the strain components $\bar{\varepsilon}_{11} = \bar{\varepsilon}_{12} = 0$ and $\bar{\varepsilon}_{22} = \varepsilon$, where $\varepsilon$ is the applied strain. The work conjugate applied stress is

$$\sigma_{ij} = \frac{1}{2(4l \cos \omega)^2} \sum \left( F_i x_j + F_j x_i \right), \tag{20}$$

where $4l \cos \omega$ is the size of the unit cell analyzed, $F_i$ is the force acting on the boundary nodes and the summation is over all these boundary nodes with coordinates $x_i$. The stress $\sigma = \sigma_{22}$ (work-conjugate to the applied strain $\bar{\varepsilon}_{22} = \varepsilon$) is evaluated in these simulations.

Finite element predictions of the effective Young's modulus of the diamond topology collinear and textile cellular materials are plotted in Figure 4(a) as a function of the relative density $\bar{\rho}$. The corresponding analytical predictions in the infinite aspect ratio limit ($A \to \infty$) are also included in Figure 4(a) and agree well with the FE predictions, especially for the collinear material. The FE and analytical predictions of the effect of the weave angle $\omega$ on the Young's modulus of a $\bar{\rho} = 0.16$ collinear and textile material is shown in Figure 4(b). The effective Young's modulus of these materials increases with increasing $\omega$ and good agreement is seen between the analytical and FE predictions.

Finite deformation FE simulations were performed to determine the peak compressive strength of the diamond topology collinear and textile cellular materials assuming elastic ideally-plastic solid wires with a yield strain $\varepsilon_y = 0.5\%$. These peak compressive strength predictions are plotted in Figure 5
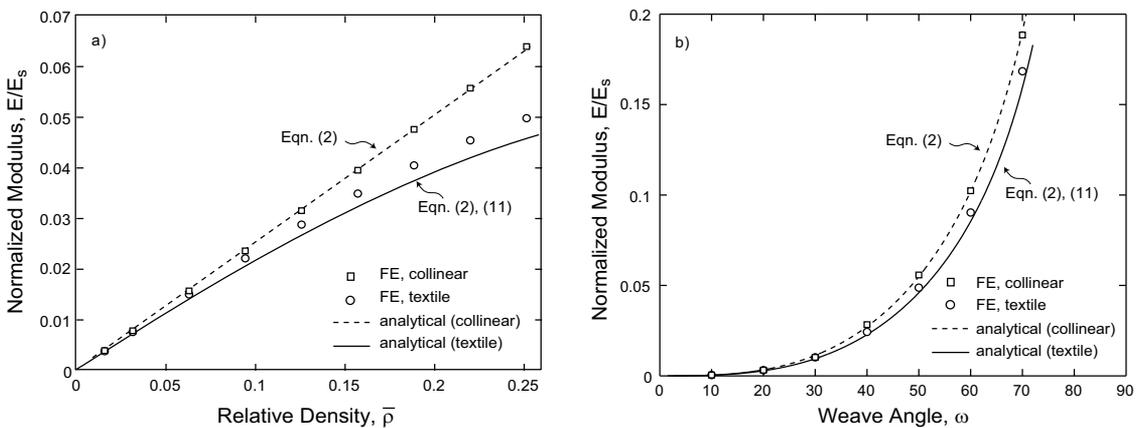


**Figure 4.** Analytical and finite element predictions of the normalized Young's modulus of the collinear and textile sandwich core materials in the diamond orientation ($A \to \infty$). (a) Effect of relative density $\bar{\rho}$ for the $\omega = \pm 45°$ diamond lattice structures and (b) the effect of the strut inclination angle $\omega$ on the modulus for $\bar{\rho} = 0.16$ lattice materials.
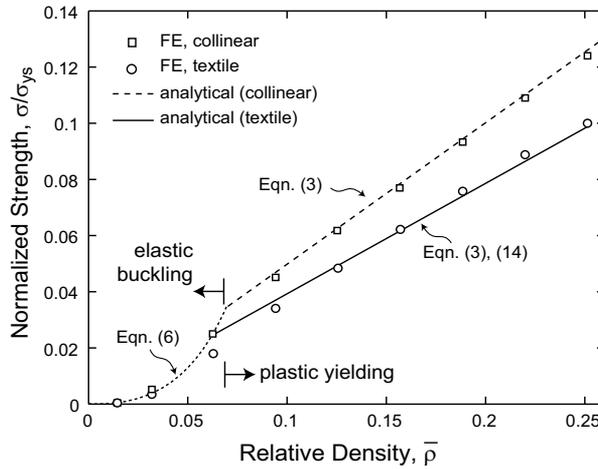
**Figure 5.** Analytical and finite element predictions of the peak compressive strength of the diamond topology collinear and textile cellular materials ($A \to \infty$) as a function of the relative density $\bar{\rho}$. The struts were assumed to be made from an elastic ideally-plastic solid with yield strain $\varepsilon_y = 0.5\%$ in these predictions.

along with the corresponding analytical estimates. For a yield strain $\varepsilon_y = 0.5\%$, elastic buckling of the constituent struts is the operative failure mode for relative densities less than approximately 0.06. The finite element calculations are in good agreement with the analytical predictions for both the collinear and textile materials in the elastic buckling as well as plastic yielding regimes.

**3.2.** *Effective properties of the material in sandwich configuration.* Finite element and analytical predictions of the Young's modulus and compressive strength of the collinear and textile materials in the
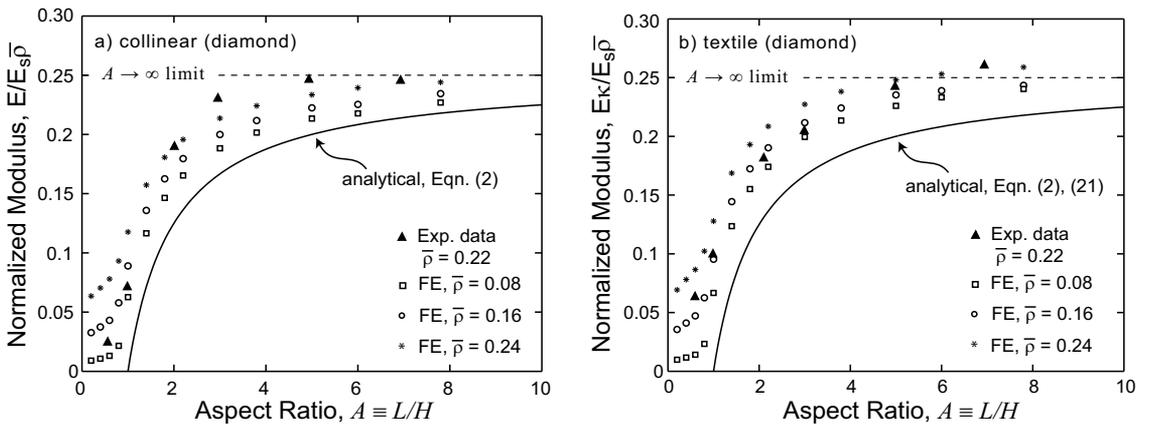


**Figure 6.** Analytical and finite element predictions of the aspect ratio dependence of the normalized Young's modulus in the diamond orientation of the (a) collinear and (b) textile sandwich core materials. Measurements on lattice materials made from 304 stainless steel are also included.

sandwich configuration are reported in this section. In all the FE calculations, a sandwich beam with 5 cells along the height $H$ of the specimen was analyzed. The specimen aspect ratio was varied by changing the specimen length $L$. All displacement and rotational degrees of freedom of the nodes along the bottom surface were completely constrained while on the top surface, a uniform compressive displacement in the $x_2$-direction was specified with the other displacement and rotational degrees of freedom constrained to zero. The work-conjugate force to the applied uniform displacement was employed to define the applied nominal stress.

Analytical and FE predictions of the variation of the normalized Young's moduli with sandwich aspect ratio $A \equiv L/H$ are plotted in Figures 6 (a) and (b) for the collinear and textile lattices, respectively. The normalization factors in Figure 6 have been chosen such that the analytical predictions give a unique curve (for all values of $\bar{\rho}$) for the collinear and textile materials. Thus, for the collinear materials we plot the normalized Young's modulus $E/(E_s\bar{\rho})$ while for the textile materials we plot $E\kappa/(E_s\bar{\rho})$, where

$$\kappa = 1.09 + 8(1+\nu)\left(\frac{a}{l}\right)^2, \tag{21}$$

is a factor due to wire waviness in the textile material, see Equation (11).

There is a rapid reduction in the normalized modulus of both collinear and textile topologies as the specimen aspect ratio $A \to 1$. It is observed that the analytical model consistently underestimates the FE predictions with the deviation between the FE and analytical predictions increasing in magnitude with higher relative densities. As previously stated, the analytical expressions assume that only struts connected to both sandwich faces carry load. However, the FE calculations indicate that struts connected to only one facesheet are able to carry load via bending at the rigidly brazed nodes. This phenomena is clearly seen in the FE predictions of the deformation of the $\bar{\rho} = 0.16$ textile sandwich lattice material with aspect ratio $A = 4$ (Figure 7). These bending effects are neglected in the analytical predictions and hence these estimates are lower than the FE predictions.

A comparison between the analytical and FE predictions of the variation of the peak compressive strength of the collinear and textile sandwich lattices as a function of aspect ratio is shown in Figures 8 (a) and (b) for relative densities of $\bar{\rho} = 0.16$ and $0.24$, respectively. Plastic yielding of the lattice trusses
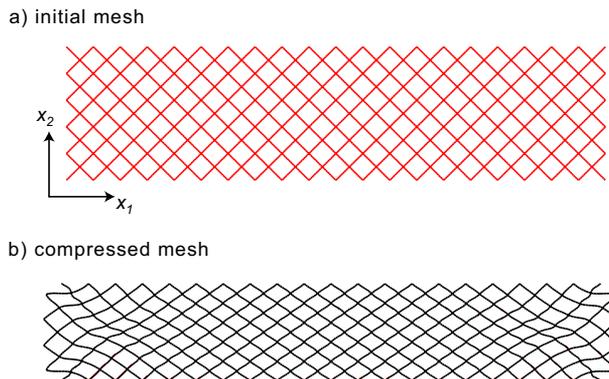


a) initial mesh

b) compressed mesh

**Figure 7.** Deformed finite element mesh for an $A = 4$, $\bar{\rho} = 0.16$ diamond topology textile sandwich core. Note that edge effects are clearly visible in the deformed mesh.

is the operative collapse mode for these relative densities and thus we have normalized the strength as $\sigma/(\sigma_{ys}\bar{\rho})$ so that the analytical predictions give a unique curve for both relative densities. Similar to the comparisons presented in Figure 6, the analytical calculations underpredict the strength, because the contribution to the strength from edge wires that carry some load by bending is neglected in those calculations. Included in Figure 8 are best fits to the FE data for aspect ratios $A > 1$. Relations of the form

$$\frac{\sigma}{\sigma_{ys}} \equiv \left(1 - \frac{0.8}{A\tan\omega}\right)\sin^2\omega \cdot \bar{\rho}, \tag{22}$$

and

$$\frac{\sigma}{\sigma_w} \equiv \left(1 - \frac{0.6}{A\tan\omega}\right)\sin^2\omega \cdot \bar{\rho}, \tag{23}$$

accurately capture the finite element predictions in Figure 8 for the collinear and textile materials, respectively.

Analogous finite element calculations also confirmed the accuracy of the simple analytical formulae presented in Section 3 for the stiffness and strength of the collinear and textile materials in the square orientation. Explicit comparisons are omitted for the sake of brevity.

## 4. Experimental assessments

The through thickness compressive stress versus strain responses of the collinear and textile sandwich lattice materials in the diamond and square orientations were examined in the experimental investigation. The compressive responses of the sandwich lattice specimens were measured at a nominal applied strain rate $4 \times 10^{-2}\,\mathrm{s}^{-1}$. The measured load cell force was used to define the nominal applied stress and the nominal through thickness strain in the lattice was estimated using a laser extensometer to monitor the relative displacements of the facesheets.
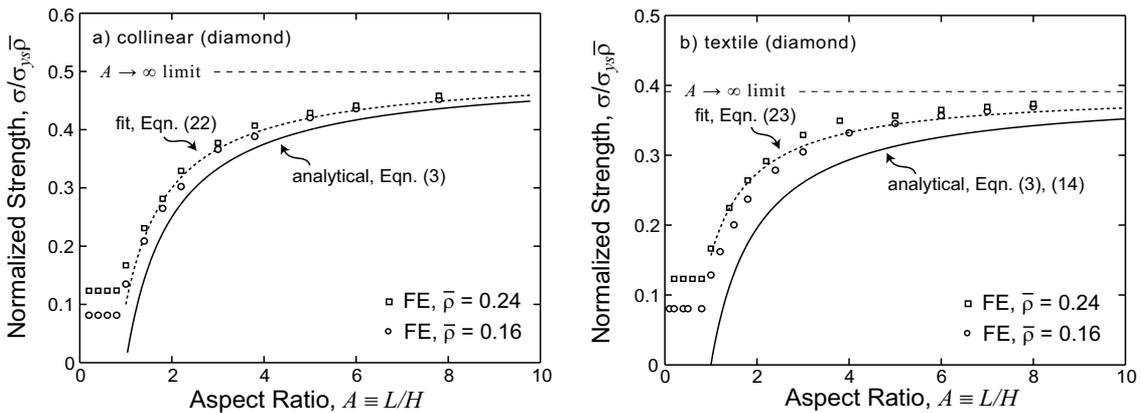


**Figure 8.** Analytical and finite element predictions of the aspect ratio dependence of the peak compressive strength in the diamond orientation of the (a) collinear and (b) textile sandwich core materials. The struts were assumed to be made from an elastic ideally-plastic solid with yield strain $\varepsilon_y = 0.5\%$ in these predictions.

**4.1.** *Materials and testing.* Schematics of the assembly method of the collinear and textile lattices made from solid 304 stainless steel wires and plain weave textiles are shown in Figure 9. These assemblies were then bonded by vacuum brazing as described by Queheillalt and Wadley [2005]. Sandwich panel specimens were produced by brazing 2.5 mm thick, 304L stainless steel sheets to the top and bottom faces of the as-cut specimens. Collinear sandwich lattice specimens were manufactured from solid 304 stainless steel wires of radius $a = 0.73$ mm spaced $l = 5$ mm apart while the textile sandwich lattices were manufactured from 304L stainless steel wire meshes of wire radius $a = 0.69$ mm and cell size $l = 5$ mm. The measured $\bar{\rho}$ for the collinear lattice was $0.23 \pm 0.005$, while the measured $\bar{\rho}$ for the textile lattice was $0.22 \pm 0.005$.

The specimens in the diamond orientation had a height $H = 21.2$ mm and width $W = 28.3$ mm. A series of through thickness compression tests on specimens with aspect ratios $0.5 \leq A \leq 7.0$ were conducted by varying the length $L$ of the specimens. The effects of both aspect ratio $A$ and height $H$ were investigated for the specimens in the square lattice orientation with $W = 29.5$ mm. The following two series of tests were conducted on the square-orientation lattices assuming similar behavior exists between the two core topologies:

- The aspect ratio dependence was investigated via a series of through thickness compression tests on textile specimens with height $H = 15$ mm and aspect ratio $A$ in the range $2.0 \leq A \leq 7.0$.

- The effect of specimen height was explored via a series of through thickness compression tests on $A = 3$ collinear specimens with heights $H$ in the range $12.3$ mm $\leq H \leq 27.3$ mm.

We note here that the width $W$ of the specimens in all cases was sufficiently large such that negligible deformation was observed in the $x_3$-direction consistent with the plane strain assumption made in the analysis reported above.

Tensile tests were conducted on the 304L stainless wires subjected to the same brazing cycle as that used to manufacture the textile and collinear sandwich lattice specimens. The measured true stress versus logarithmic strain response revealed that the parent material is adequately approximated as an
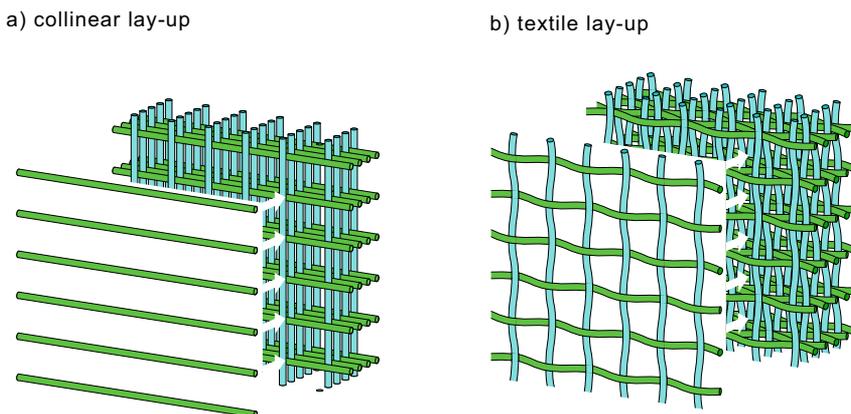
a) collinear lay-up    b) textile lay-up

**Figure 9.** Sketches illustrating the manufacture of the (a) collinear and (b) textile cores.
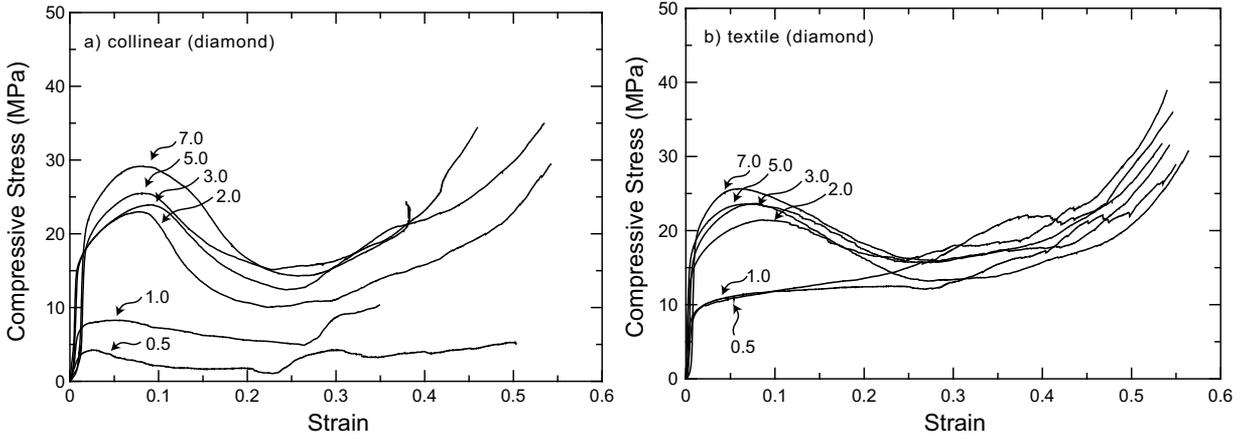
**Figure 10.** Measured compressive stress versus strain responses of (a) the $\bar{\rho} = 0.23$ collinear and (b) the $\bar{\rho} = 0.22$ textile diamond oriented cellular sandwich cores. Results are plotted for selected values of the specimen aspect ratio, $A$.

elastic-plastic solid with Young's modulus $E_s = 200\,\text{GPa}$, 0.2% offset yield strength $\sigma_{ys} = 189\,\text{MPa}$ and a linear hardening modulus $E_t \equiv d\sigma/d\varepsilon \approx 2450\,\text{MPa}$.

## 4.2. *Results and discussion.*

**4.2.1.** *Diamond orientation.* The through thickness nominal compressive stress versus nominal strain responses of the diamond topology collinear and textile lattices are plotted in Figure 10 for samples with aspect ratios $0.5 \leq A \leq 7.0$. The modulus was measured via unload/reload curves within the elastic loading regime and are plotted versus aspect ratio in Figure 6. (The unload/reload modulus portions
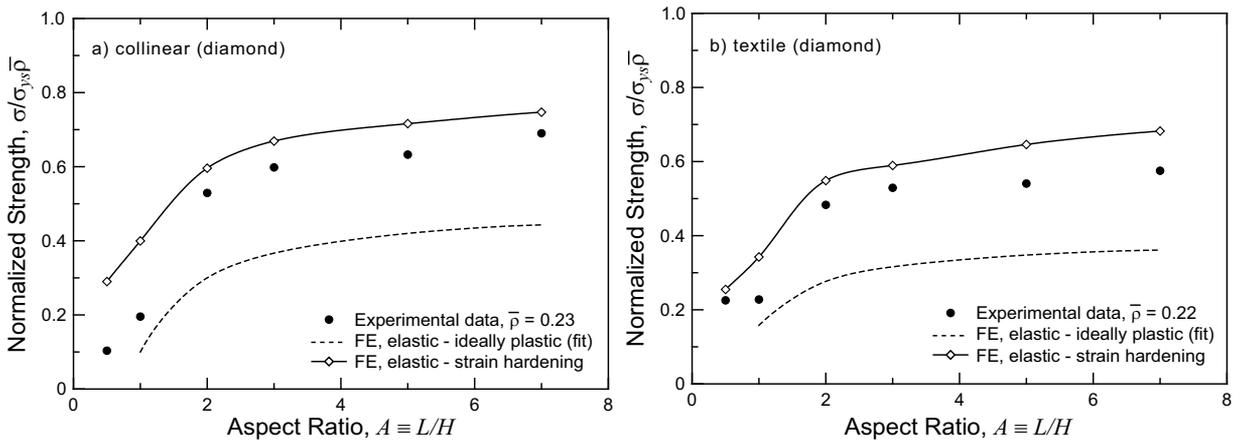


**Figure 11.** Finite element predictions and measured values of the peak compressive strengths for the diamond orientation (a) $\bar{\rho} = 0.23$ collinear and (b) the $\bar{\rho} = 0.22$ textile sandwich core materials. Also included are the fits (Equations (22) and (23)) derived from the ideally-plastic finite element simulations.

of the stress-strain curves were removed from Figure 10 for the sake of clarity.) The measured Young's moduli agree well with FE predictions while the analytical calculations slightly underpredict the stiffness because bending of the edge wires is neglected in the analytical estimates.

The peak compressive strength of both the collinear and textile lattices is plotted in Figure 11 as a function of the specimen aspect ratio $A$. The peak compressive strength of both diamond lattices increases with increasing specimen aspect ratio. The peak strength was achieved at compressive strains in the range 5% to 10% indicating that the peak strengths of these stainless steel cellular material are governed by plastic buckling of the constituent wires with the strain hardening of the 304 stainless steel playing a significant role.

Finite element simulations of these experiments were repeated using a solid material having the measured characteristics of the as-brazed 304L stainless steel. A comparison between the strain hardening finite element predictions and the measured peak compressive strength values is shown in Figure 11 for the two diamond lattices. Also included in Figure 11 are the elastic perfectly-plastic FE estimates (Equations (22) and (23)) using $\sigma_{ys} = 189$ MPa. Good agreement between the measurements and strain hardening FE predictions (especially for $A > 1$) are observed whereas the ideally plastic simulations significantly underpredict the peak strength at the highest aspect ratios. This confirms our expectation that the strain hardening of the 304 stainless steel plays a significant role in establishing the peak strength of these cellular materials. Note that some deviation is seen for $A < 1$. This is due to the FE simulation assuming a perfectly rigid bond between nodes, whereas the brazed joint has a lower strength than the parent material: node fractures were observed especially in the specimens with aspect ratios $A < 1$.

**4.2.2.** *Square orientation.* The through thickness compressive nominal stress versus nominal strain responses of the square lattices are shown in Figure 12. In Figure 12(a), the compressive responses of collinear cores with an aspect ratio $A = 3$ are shown for three sandwich core heights, $H$. In Figure 12(b), the effect of aspect ratio on the stress versus strain responses of the square textile lattices is investigated
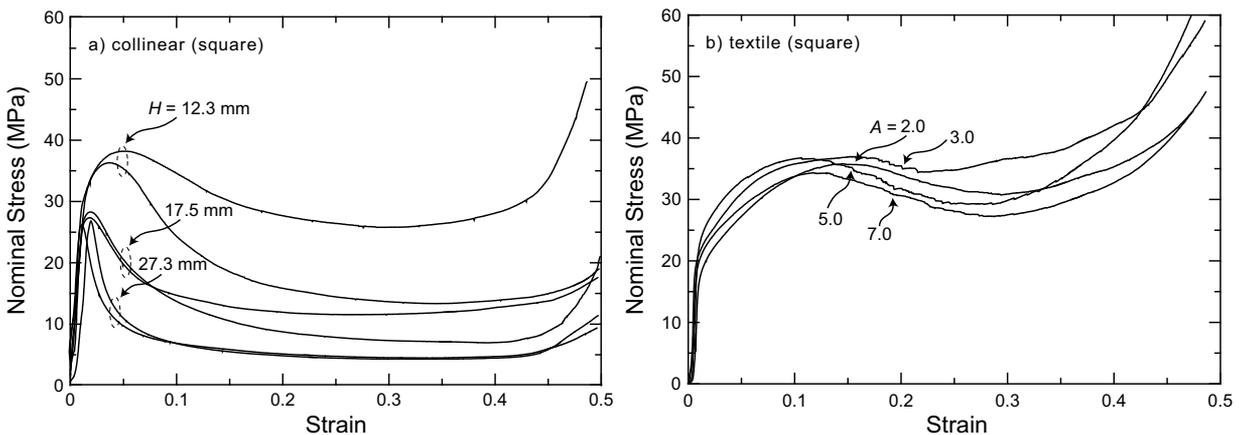


**Figure 12.** Measured compressive stress versus strain responses of (a) the $\bar{\rho} = 0.23$ collinear ($A = 3.0$) and (b) the $\bar{\rho} = 0.22$ textile square oriented ($H = 15.0$ mm) cellular sandwich core materials.
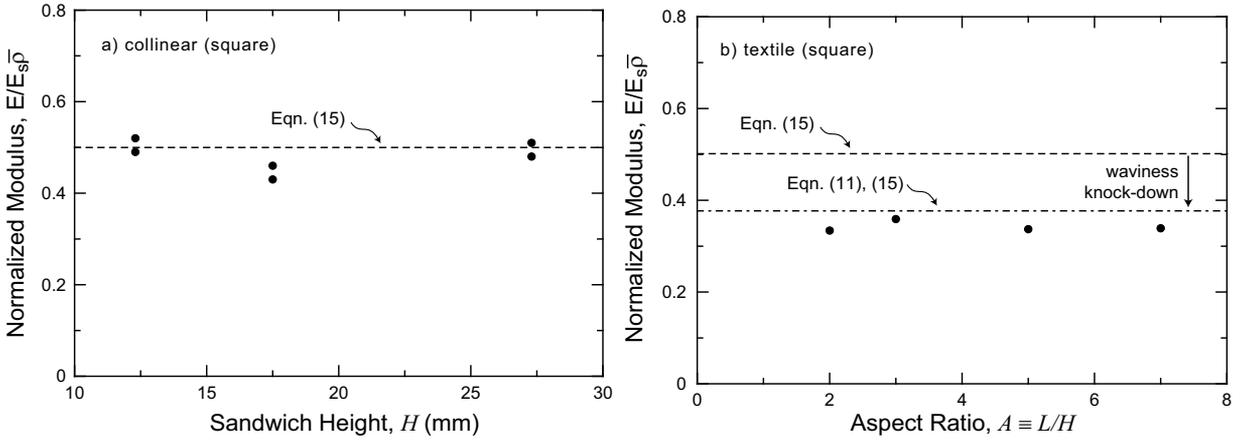
**Figure 13.** Analytical predictions and measured values of the normalized Young's modulus for the (a) $\bar{\rho} = 0.23$ square collinear and (b) the $\bar{\rho} = 0.22$ square textile sandwich core materials as a function of specimen height $H$ and aspect ratio $A$, respectively.

for a specimen height $H = 15.0$ mm. The peak compressive strength of the square collinear lattice is seen to decrease with increasing core height while the specimen aspect ratio has a negligible effect.

The effective Young's moduli were evaluated from unload/reload cycles prior to the onset of plastic yielding of the square lattices. This data is plotted in Figure 13(a) as a function of sample height $H$ and in Figure 13(b) as a function of sample aspect ratio $A \equiv L/H$. The analytical predictions are included as dashed horizontal lines in both figures. The analytical predictions are in good agreement with the square collinear lattice data. A significant knock-down in the modulus of the textile material compared to that of the collinear material was observed, and this *waviness* effect is well predicted by Equation (11).
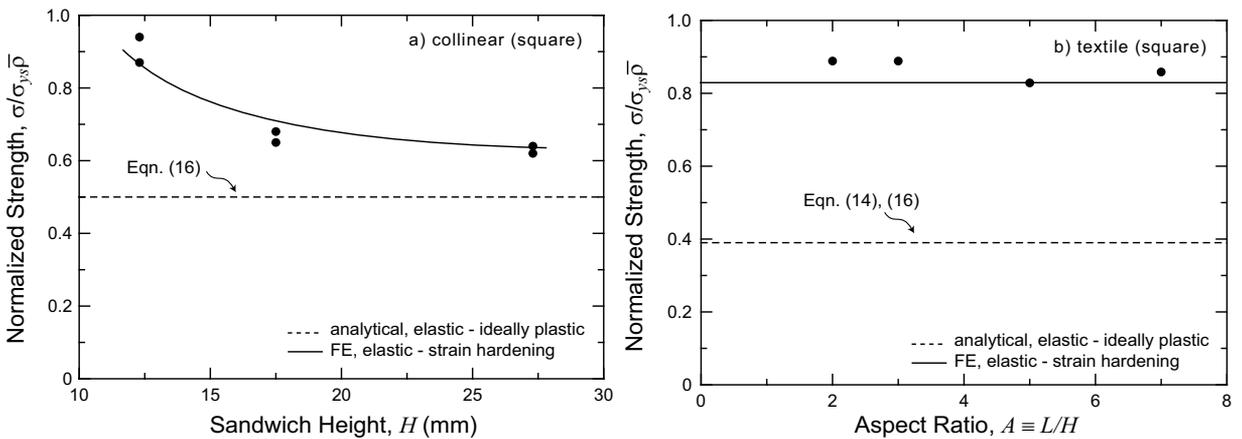


**Figure 14.** Analytical and FE predictions and measured values of the normalized compressive strengths for the (a) $\bar{\rho} = 0.23$ square collinear and (b) $\bar{\rho} = 0.22$ square textile sandwich core materials as a function of specimen height $H$ and aspect ratio $A$, respectively.

The variation of the peak compressive strength of the $A = 3$ square collinear sandwich core with core height $H$ is plotted in Figure 14(a). The normalized peak strengths $\sigma/(\sigma_{ys}\bar{\rho})$ exceed 0.5 which indicates that plastic buckling is the operative collapse mode in this case. Finite element predictions (which include the strain hardening of the 304 stainless steel) of the peak strengths are also included in Figure 14(a) and agree well with the experimental measurements. Experimental measurements and FE as well as analytical predictions of the peak strengths for the $H = 15$ mm square textile lattice are compared in Figure 14(b) for specimen aspect ratios in the range $2.0 \leq A \leq 7.0$. Again, plastic buckling is the operative collapse mode (the normalized peak strength $\sigma/(\sigma_{ys}\bar{\rho})$ exceeds 0.5) and the FE predictions with material strain hardening included agree well with the measurements.

## 5. Conclusions

Metallic cellular materials are manufactured by laying-up either collinear arrays of solid wires (alternating the direction of successive layers) or woven (textile) meshes. These two routes result in similar lattice truss topologies which differ in the fact that the collinear lattice comprises straight struts while the corresponding struts in the textile material are wavy. Analytical and finite element (FE) calculations show that waviness of the struts results in about a 20% reduction in the stiffness and strength of the textile lattice materials compared to the corresponding collinear materials.

Through-thickness compression tests were conducted on the collinear and textile cores in the diamond and square orientations. In the diamond orientation the stiffness and strength are sensitive to the specimen aspect ratio for aspect ratios less than about 4. By contrast, the properties of sandwich cores in the square orientation are reasonably independent of the specimen aspect ratio but the strength decreases with increasing core height due to buckling of the wires across the entire height of the sandwich core. This mode is suppressed in the diamond orientation and thus the diamond orientation is considered more useful from a practical standpoint.

## References

[Ashby et al. 2000] M. F. Ashby, T. Evans, N. A. Fleck, L. J. Gibson, J. W. Hutchinson, and H. N. G. Wadley, *Metal foams: a design guide*, Butterworth-Heinemann, Boston, 2000.

[Berggren et al. 2001] S. A. Berggren, D. Lukkassen, A. Meidell, and L. Simula, "On stiffness properties of square honeycombs and other unidirectional composites", *Compos. B Eng.* **32**:6 (2001), 503–511.

[Bitzer 1997] T. N. Bitzer, *Honeycomb technology: materials, design, manufacturing, applications and testing*, Chapman & Hall, London, 1997.

[Buannic et al. 2003] N. Buannic, P. Cartraud, and T. Quesnel, "Homogenization of corrugated core sandwich panels", *Compos. Struct.* **59**:3 (2003), 299–312.

[Chen et al. 1999] C. Chen, T. J. Lu, and N. A. Fleck, "Effect of imperfections on the yielding of two-dimensional foams", *J. Mech. Phys. Solids* **47**:11 (1999), 2235–2272.

[Cote et al. 2004] F. Cote, V. S. Deshpande, N. A. Fleck, and A. G. Evans, "The out-of-plane compressive behavior of metallic honeycombs", *Mater. Sci. Eng. A* **380**:1-2 (2004), 272–280.

[Cote et al. 2006] F. Cote, V. S. Deshpande, N. A. Fleck, and A. G. Evans, "The compressive and shear responses of corrugated and diamond lattice materials", *Int. J. Solids Struct.* **43**:20 (2006), 6220–6242.

[Deshpande and Fleck 2001] V. S. Deshpande and N. A. Fleck, "Collapse of truss core sandwich beams in 3-point bending", *Int. J. Solids Struct.* **38**:36-37 (2001), 6275–6305.

[Gibson and Ashby 1997] L. J. Gibson and M. F. Ashby, *Cellular solids: structure and properties*, 2nd ed., Cambridge solid state science series, Cambridge University Press, Cambridge, 1997.

[Grenestedt 1998] J. L. Grenestedt, "Influence of wavy imperfections in cell walls on elastic stiffness of cellular solids", *J. Mech. Phys. Solids* **46**:1 (1998), 29–50.

[Grenestedt and Bassinet 2000] J. L. Grenestedt and F. Bassinet, "Influence of cell wall thickness variations on elastic stiffness of closed-cell cellular solids", *Int. J. Mech. Sci.* **42**:7 (2000), 1327–1338.

[Grenestedt and Tanaka 1998] J. L. Grenestedt and K. Tanaka, "Influence of cell shape variations on elastic stiffness of closed cell cellular solids", *Scripta Mater.* **40**:1 (1998), 71–77.

[Hyun et al. 2003] S. Hyun, A. M. Karlsson, S. Torquato, and A. G. Evans, "Simulated properties of Kagomé and tetragonal truss core panels", *Int. J. Solids Struct.* **40**:25 (2003), 6989–6998.

[Kooistra et al. 2004] G. W. Kooistra, V. S. Deshpande, and H. N. G. Wadley, "Compressive behavior of age hardenable tetrahedral lattice truss structures made from aluminium", *Acta Mater.* **52**:14 (2004), 4229–4237.

[Liang and Chen 2006] S. Liang and H. L. Chen, "Investigation on the square cell honeycomb structures under axial loading", *Compos. Struct.* **72**:4 (2006), 446–454.

[Meidell 2005] A. Meidell, "On some new formulae for in-plane elastic moduli of square honeycomb structures", *Int. J. Comput. Civil Struct. Eng.* **1**:1 (2005), 79–88.

[Noor et al. 1995] A. K. Noor, W. S. Burton, and C. W. Bert, "Computational model for sandwich panels and shells", *Appl. Mech. Rev.* **155** (1995), 155–199.

[Prager 1959] W. Prager, *An introduction to plasticity*, Addison-Wesley, Reading, MA, 1959.

[Queheillalt and Wadley 2005] D. T. Queheillalt and H. N. G. Wadley, "Cellular metal lattices with hollow trusses", *Acta Mater.* **53**:2 (2005), 303–313.

[Simone and Gibson 1998a] A. E. Simone and L. J. Gibson, "The effects of cell face curvature and corrugations on the stiffness and strength of metallic foams", *Acta Mater.* **46**:11 (1998), 3929–3935.

[Simone and Gibson 1998b] A. E. Simone and L. J. Gibson, "Effects of solid distribution on the stiffness and strength of metallic foams", *Acta Mater.* **46**:6 (1998), 2139–2150.

[Sypeck and Wadley 2001] D. J. Sypeck and H. N. G. Wadley, "Multifunctional microtruss laminates: textile synthesis and properties", *J. Mater. Res.* **16**:3 (2001), 890–897.

[Sypeck and Wadley 2002] D. J. Sypeck and H. N. G. Wadley, "Cellular metal truss core sandwich structures", *Adv. Eng. Mater.* **4**:10 (2002), 759–764.

[Valdevit et al. 2004] L. Valdevit, J. W. Hutchinson, and A. G. Evans, "Structurally optimized sandwich panels with prismatic cores", *Int. J. Solids Struct.* **41**:18-19 (2004), 5105–5124.

[Wadley et al. 2003] H. N. G. Wadley, N. A. Fleck, and A. G. Evans, "Fabrication and structural performance of periodic cellular metal sandwich structures", *Compos. Sci. Technol.* **63**:16 (2003), 2331–2343.

[Wallach and Gibson 2001] J. C. Wallach and L. J. Gibson, "Defect sensitivity of 3D truss material", *Scripta Mater.* **45**:6 (2001), 639–644.

[Wang et al. 2003] J. Wang, A. G. Evans, K. Dhamasena, and H. N. G. Wadley, "On the performance of truss panels with Kagomé cores", *Int. J. Solids Struct.* **40**:25 (2003), 6981–6988.

[Zok et al. 2004] F. W. Zok, S. A. Waltner, Z. Wei, H. J. Rathbun, R. M. McMeeking, and A. G. Evans, "A protocol for characterizing the structural performance of metallic sandwich panels: application to pyramidal truss cores", *Int. J. Solids Struct.* **41**:22-23 (2004), 6249–6271.

[Zupan et al. 2004] M. Zupan, V. S. Deshpande, and N. A. Fleck, "The out-of-plane compressive behaviour of woven-core sandwich plates", *Eur. J. Mech. A Solid* **23**:3 (2004), 411–421.

DOUGLAS T. QUEHEILLALT: dougq@virginia.edu
*Department of Materials Science and Engineering, University of Virginia, 140 Chemistry Way, Charlottesville, VA 22904, United States*

VIKRAM S. DESHPANDE: vsd@engineering.ucsb.edu
*Department of Mechanical Engineering, University of California, Santa Barbara, Santa Barbara, CA 93106, United States*

HAYDN N. G. WADLEY: haydn@virginia.edu
*Department of Materials Science and Engineering, University of Virginia, 140 Chemistry Way, Charlottesville, VA 22904, United States*